

MG-MixF PPP-AR User Manual

Multi-GNSS and Mixed Multi-frequency

Precise Point Positioning Ambiguity

Resolution software

written by Zhiguo Sun, Fuxin Yang

Email: sun_zhiguo@hebeu.edu.cn
yangfuxin@hrbeu.edu.cn

Last modified: Feb 2, 2024



**College of Intelligent Systems Science and Engineering,
Harbin Engineering University**

Contents

1 Introduction.....	1
2 Supported platforms.....	1
3 Installation	2
3.1 Install Qt	2
3.3 Run MG-MixF PPP-AR with executable program.....	4
4 Filter Parameter configuration.....	5
5 Position Mode configuration.....	5
6 GNSS data processing.....	9
6.1 Single station processing.....	9
6.2 Multiple station processing	10
6.3 Multi-day data processing	11
7 Result and analysis.....	12
7.1 position.txt and back_position.txt	12
7.2 Ambiguity_information.txt and back_Ambiguity_information.txt	12
7.3 dop_satN_AR.txt and back_dop_satN_AR.txt.....	14
7.4 Az_El_coff.txt and back_Az_El_coff.txt	14
7.5 ZTDW_Clock.txt and back_ZTDW_Clock.txt	15
7.6 bad_satellites.txt and back_bad_satellites.txt	15
7.7 Satellite_info.txt and back_Satellite_info.txt.....	15
8 Thanks & Support	16
Appendix.....	17
A. Data processing models and strategies of MG-MixF PPP-AR.....	17
B. The urban and ocean Kinematic Experiment.....	18

1 Introduction

The open-source MG-MixF PPP-AR is developed based on the GUN General Public License version 3 (GPLv3) protocol, and includes all of the C++ and Qt source code. The software provides a rich function library that makes subsequent development easier, and can run on UNIX/Linux, Windows, and other operating systems. MG-MixF PPP-AR supports mixed dual- and tri-frequency uncombined PPP AR using AR products from WHU and CNES. In addition, the toolbox is compatible with the conventional dual-frequency multi-GNSS IF combined PPP AR. It provides not only a user-friendly HMI, but also the ability to batch process multi-day and multi-station data to produce high-precision PPP AR results. Thus, it meets the diverse research and application needs of users. MG-MixF PPP-AR must have the required products available under the user selected catalogue when performing dual- or triple-frequency or mixed dual- and triple-frequency uncombined PPP-AR. During data processing, it can process the data using SRIF or Kalman filtering algorithms.

2 Supported platforms

The MG-MixF PPP-AR software was developed in the C++ language based on the cross-platform Qt framework. It can be compiled and executed on popular operating systems such as Windows, UNIX/Linux, Mac, and other operating systems. It is recommended to debug MG-APP under Qt Creator in UNIX/Linux or Windows system.

Computer configuration requirements as follows:

Operating system: Linux or Windows

System type: 32 or 64 bit

Memory: at least 512MB

Hard disk space: hard disk at least 500MB

Qt Version: Qt version higher than 5.7.0

All the operation examples and the performance of the software demonstrated in the following content are recorded under the Windows 10 system, including software installation and testing. The software was also tested under the Ubuntu system with the

version equal to 16.04 or higher, and the tests passed.

3 Installation

3.1 Install Qt

You can compile the source code of MG-MixF PPP-AR with QT, as follows:

Users need to install Qt5.14.2 from Qt official website (www.qt.io) to open project and recompile to generate the required executable program under operating system. QT installation packages for different platforms are published on QT official website (www.qt.io). If you use Windows system, please choose: <https://download.qt.io/archive/qt/5.14/5.14.2/qt-opensource-windows-x86-5.14.2.exe>. If you use Linux system, choose: <https://download.qt.io/archive/qt/5.14/5.14.2/qt-opensource-linux-x64-5.14.2.run>. When you install Qt5.14.2, you need to choose MinGW 7.3.0 32bit based on your operating system. As shown in Fig. 1.



Fig. 1 Choose MinGW depending on operating system

3.2 Compile MG-MixF PPP-AR from source code

After the installation of Qt is finished, user can open the Qt Creator and click the menu

bar "File->Open File or Project..." to open " MG-MixF PPP-AR.pro" in the source folder MG-MixF PPP-AR, and you will see the window shown in Fig. 2 (Qt Creator has a uniform interface in Windows, UNIX/Linux, and other operating systems). MG-MixF PPP-AR can be compiled and run after the triangular button has been clicked.

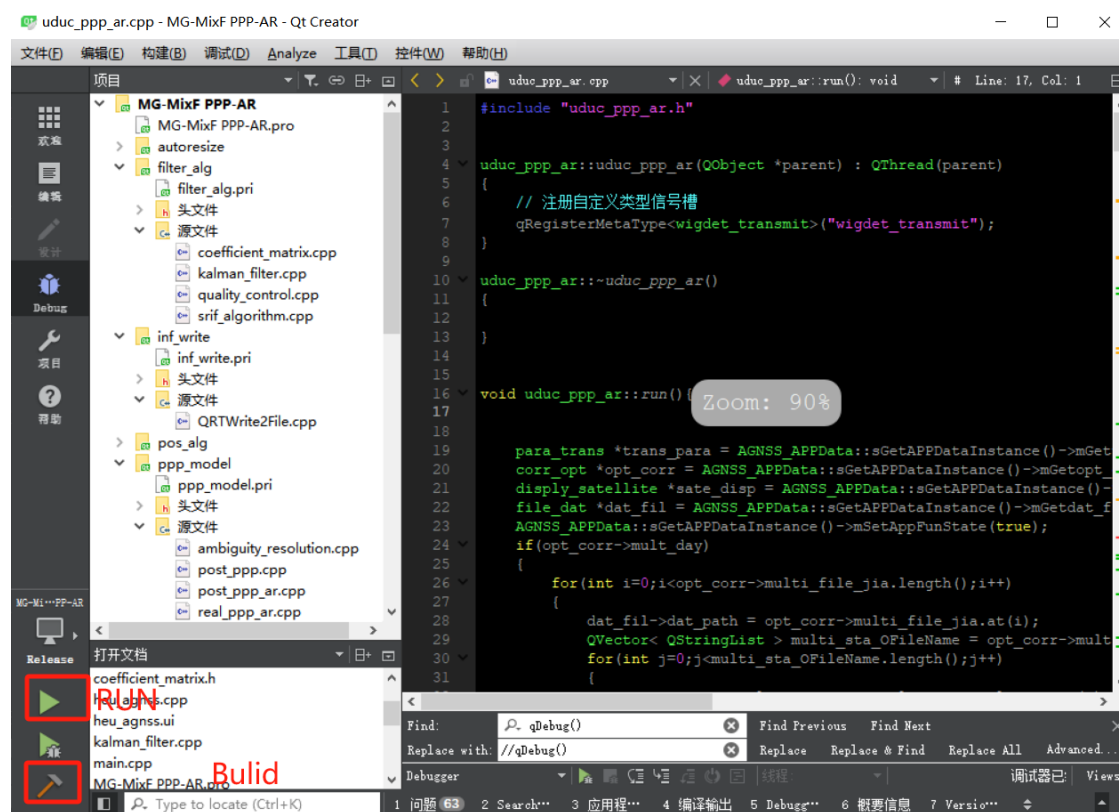


Fig. 2 The Qt window in Win10 system

The files to be copied are placed in “MinGW_32bit-CopyData” under “MG-MixF PPP AR\resources”, as follows

MG-MixF PPP-AR > resources > MinGW_32bit-CopyData				在 MinGW_32bit-Co...
名称	修改日期	类型	大小	
MG-MixF Config.ini	2024/12/4 19:40	配置设置	2	
MG-MixF Config.json	2024/12/4 19:40	JSON 文件	2	
MG-MixF PPP-AR.ini	2024/12/4 19:40	配置设置	1	
MG-MixF PPP-AR.json	2024/12/4 19:40	JSON 文件	1	

Fig. 3 Files with configuration information

After clicking "Run" button in Fig. 2 the main window of MG-MixF PPP-AR will appear as shown in Fig. 4.

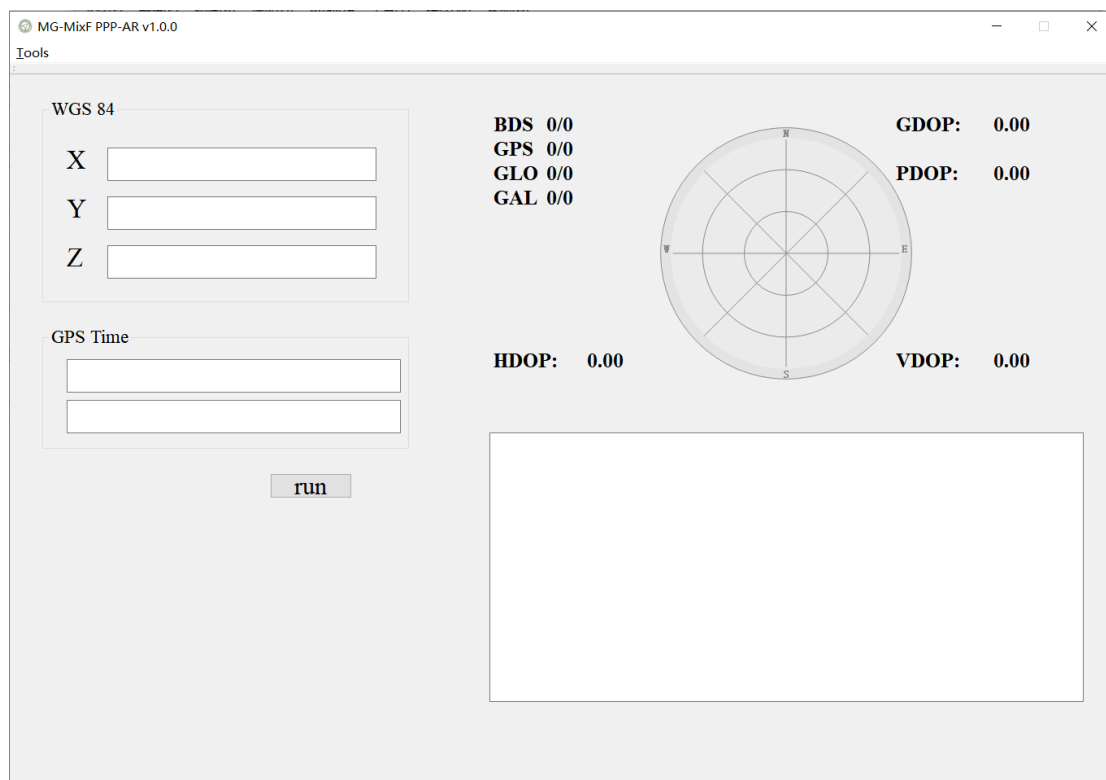


Fig. 4 The MG-MixF PPP AR window

3.3 Run MG-MixF PPP-AR with executable program

MG-MixF.exe in the release folder is moved to the “MG-MixF PPP AR V1.0.0” folder. Then ‘cd’ to the “bin” folder and ‘windeployqt.exe’ MG-MixF.exe in “Qt 5.14.2(MinGW 7.3.0 32-bit)”.

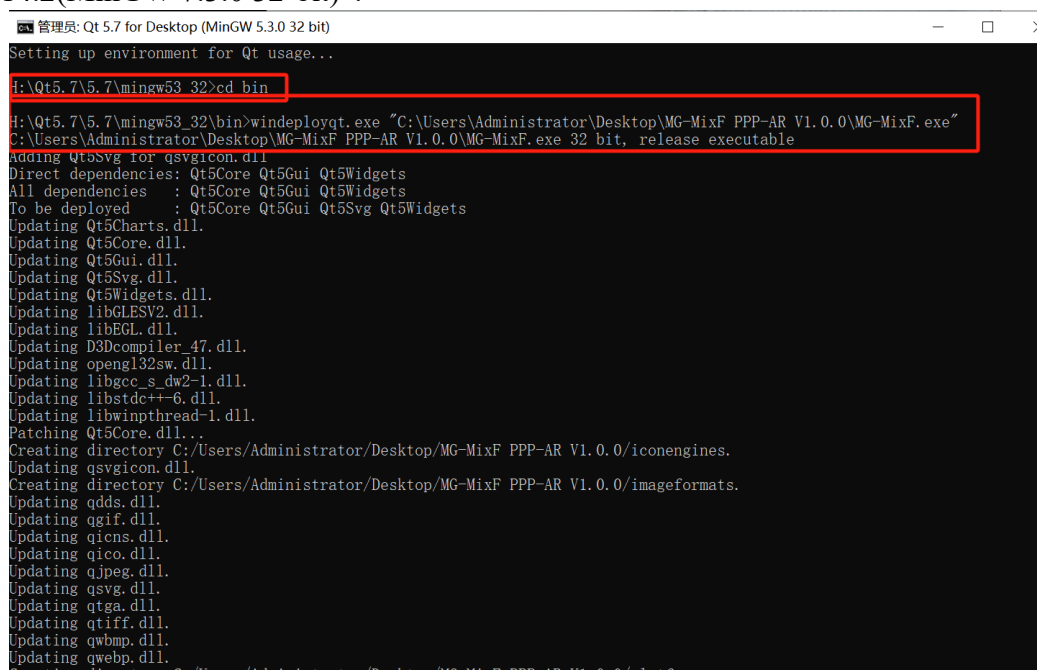


Fig. 5 Qt packaged executable MG-MixF.exe

Copy the files in the folder " MG-MixF PPP AR\resources" to the folder " MG-MixF

PPP AR V1.0.0". Double click on MG-MixF.exe in the " MG-MixF PPP AR V1.0.0" folder with the left mouse button to get the same interface as Fig. 4.

4 Filter Parameter configuration

The filter parameters can be configured by clicking the "configure" button in the tools drop-down box in the upper left corner of the MG-MixF PPP AR software, as shown in Fig. 6. In Fig. 6, the parameters in the **red boxes** are the contents of the parameters of the future open source programme and do not need to be adjusted.

ConfigWidget

Set Parameters($m^2/30s$)

	dynamic_pos	zwd	clk	amb	ion
Transfer noise (Qw):	1e4	3e-8	1e6	1e-16	0.1
Initial covariance (Pk):	1e3	10	1e6	1e6	10
Carrier/Pseudorange precision (m):G		0.03	3.0		
Carrier/Pseudorange precision (m):C2		0.03	3.0	C3 0.03	3.0
Carrier/Pseudorange precision (m):E		0.03	3.0	R 0.03	3.0

Helmert variance covariance estimation

☐ Helmert VC select

WL/EWL fixed ambiguity w

1e6

NL ambiguity cutoff

0.5

stochastic model

Weighted sine elevation angle

Ratio Test

Ratio value: 2.0

Ok Cancel

Fig. 6 Parameter Configuration Interface

5 Position Mode configuration

Left-click on 'Tools' in Fig. 4 and select 'SetWidget' to display the position information configuration as shown in Fig. 7. In Fig. 7, you can configure the positioning mode, data output content, multi-station data processing, quality control mode, filter mode, processing data path, result storage path, and so on.

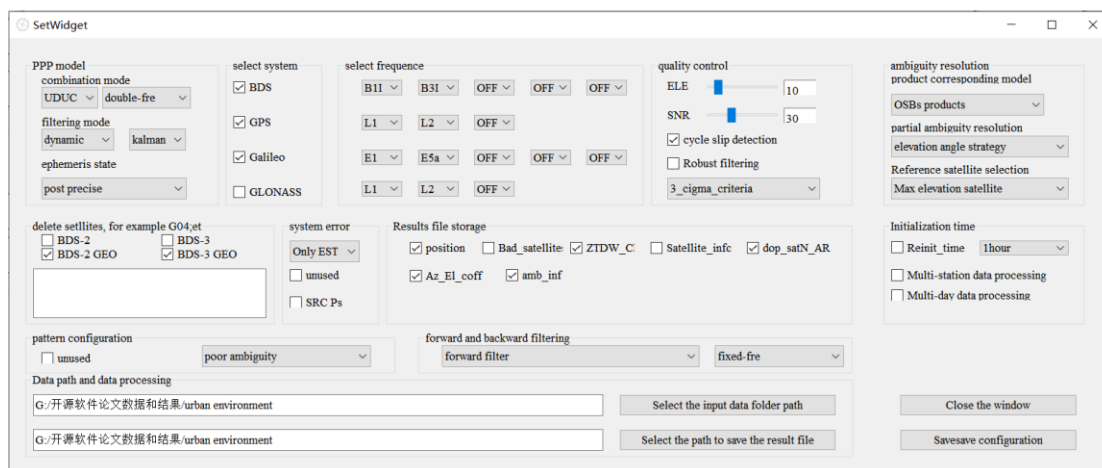


Fig. 7 Position information configuration

The positioning model configuration allows for the selection of ‘UDUC’ (Undifferentiated Uncombined Mode) or ‘IF’ (Ionosphere Free Combined Mode) as shown Fig. 8. The frequency selection is shown in Fig. 9. The static positioning or dynamic positioning selection is shown in Fig. 10.

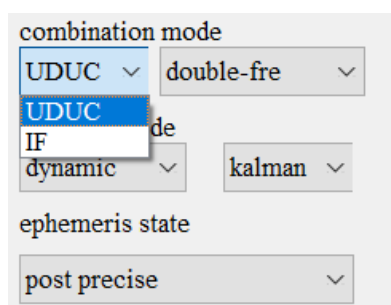


Fig. 8 Select Positioning Mode

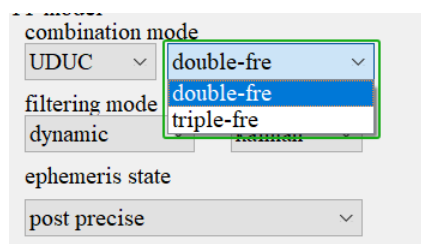


Fig. 9 Select Observation frequency

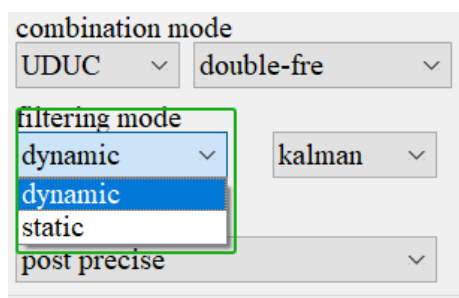


Fig. 10 Select positioning mode

The selection of mixed multi-frequency models is shown in Fig. 11.

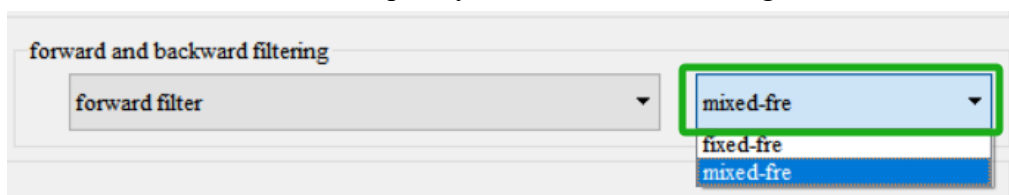


Fig. 11 Select mixed frequency model

The selection of satellite systems involved in positioning and the selection of frequencies for the dual-frequency 'UDUC' model are shown in Fig. 12.

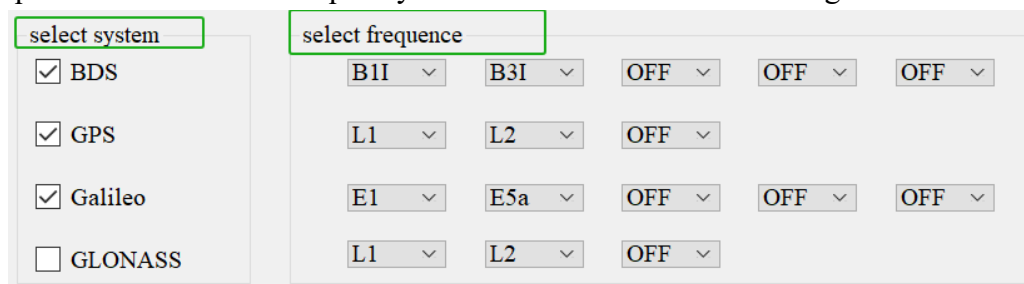


Fig. 12 Select system and dual-frequency

The selection of frequencies for the tri-frequency 'UDUC' model is shown in Fig. 13.

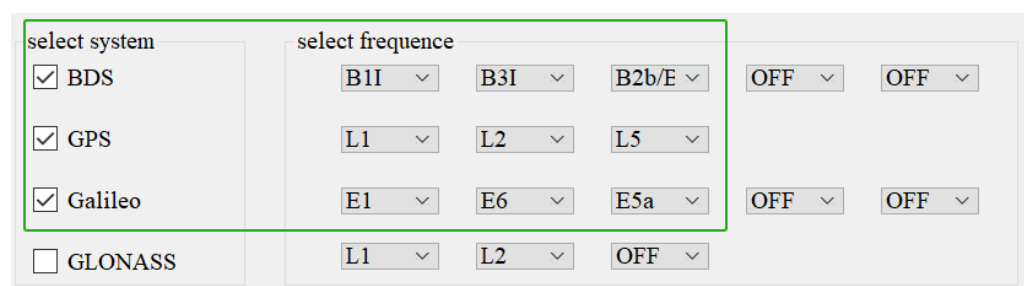


Fig. 13 Select system and tri-frequency

In Fig. 14 'OSBs products' is the ambiguity fixed solution PPP mode using OSB products, 'Float solution' is the ambiguity float solution PPP mode, the 'Integer clock products' is the ambiguity fixed solution PPP mode for integer clock products and 'UPD/FCBs products' is the ambiguity fixed solution PPP mode for FCB products.

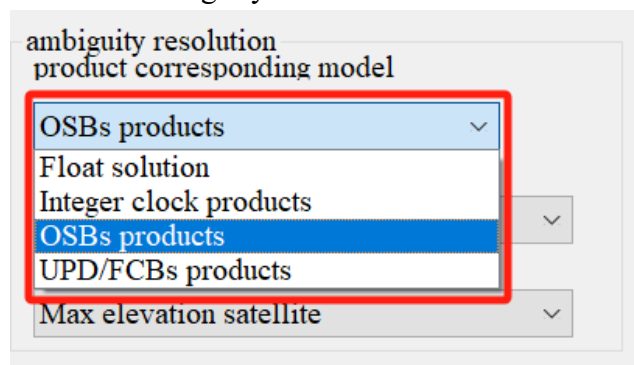


Fig. 14 Select Ambiguity Resolution mode

In Fig. 15, 'elevation angle strategy' is the partial ambiguity fixed mode using elevation angle, 'success rate criterion' is the ambiguity excluded mode using bootstrapping

success rate, 'full ambiguity fixed' is the full ambiguity fixed mode, and 'posterior residual sequence' is the a posteriori residual exclusion of carrier phase observations. partial ambiguity fixed mode, 'full ambiguity fixed' for full ambiguity fixed mode, 'posterior residual sequence' for carrier phase observation a posteriori residual exclusion partial ambiguity fixed mode for ambiguity, 'ADOP ' for partial ambiguity fixed mode for carrier phase observation a posteriori residual exclusion ambiguity.

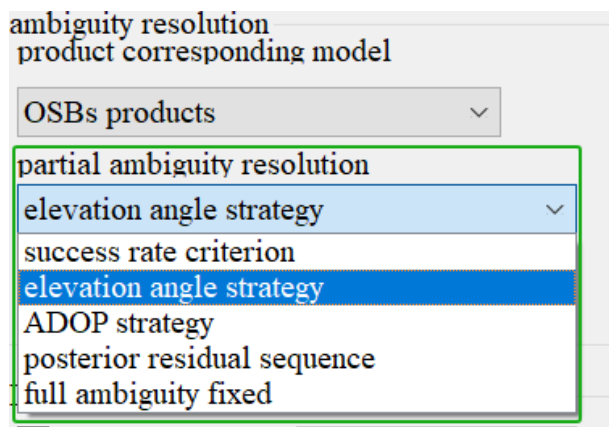


Fig. 15 Select Partial Ambiguity fixed mode

The selection of the filter filtering direction is shown in Fig. 16.

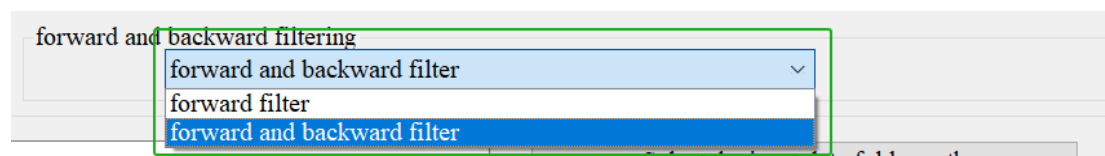


Fig. 16 Select the filter direction

The data path selection and the result file storage path selection are shown in Fig. 17.

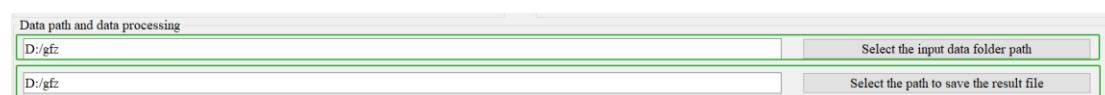


Fig. 17 Select data path

The Delete Satellite panel is shown in Fig. 18.

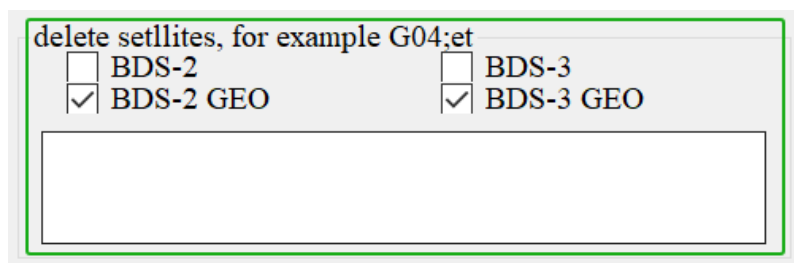


Fig. 18 Delete Satellite Panel

The error estimation method between the selected satellite systems is shown in Fig. 19.

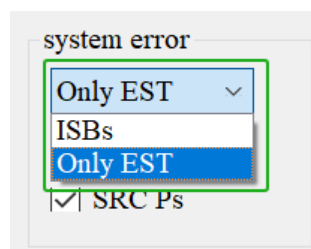


Fig. 19 Selection of error estimation method between satellite systems

The selection of the output result file is shown in Fig. 20.

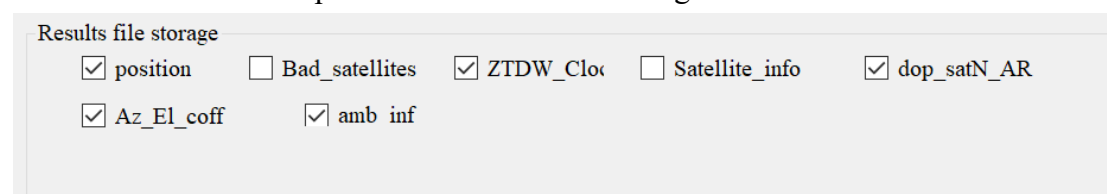


Fig. 20 Select the output result file

Multi-day, multi-station data selection and initialisation time selection are shown in Fig. 21.

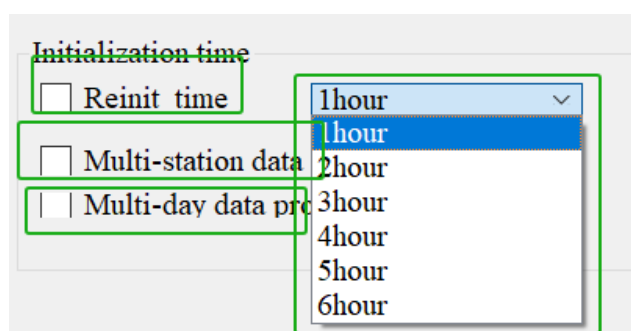


Fig. 21 Multi-day, multi-station and initialisation time selection

6 GNSS data processing

6.1 Single station processing

This section mainly introduces the operation of single station data processing by MG-MixF PPP-AR. Firstly, the observation file (*.o) to a new folder (e.g., D/single station processing). Then, the precision clock file (*.CLK), the precision orbit file (*.SP3), the OSB product file (*.BIA), the satellite attitude file (*.OBX), and the antenna file (*.atx) are copied to the same folder as the observation file, as shown in Fig. 22. Click the button "Run " in Fig. 4 to process data of single stations. The MG-MixF PPP AR software runs as shown in Fig. 23. The list of generated files is shown in Fig. 24.

名称	修改日期	类型	大小
CEBR00ESP_R_20230380000_01D_30S_MO.23o	2023/8/21 14:02	23O 文件	35,708 KB
GBM0MGXRAP_20230380000_01D_05M_ORB.SP3	2023/2/13 17:45	SP3 文件	2,919 KB
GBM0MGXRAP_20230380000_01D_30S_ABS.BIA	2023/2/13 23:53	BIA 文件	252,112 KB
GBM0MGXRAP_20230380000_01D_30S_ATT.OBX	2023/2/13 17:45	OBX 文件	36,984 KB
GBM0MGXRAP_20230380000_01D_30S_CLK.CLK	2023/2/13 17:45	CLK 文件	24,263 KB
igs20_2221.atx	2023/2/13 17:45	ATX 文件	31,428 KB

Fig. 22 Single-station data-processing preparation files

Fig. 23 PPP AR processing using MG-MixF PPP AR

Sample Data > post_2023032 > OSBs_BRUX_Mixed_UC_Kalman_Triple_PPP_GEC_KINEMATIC_2024-12-05_10_40_14_966			
名称	修改日期	类型	大小
Ambiguity_information.txt	2024/12/5 10:42	文本文档	11,146 KB
Az_El_coff.txt	2024/12/5 10:42	文本文档	4,507 KB
dop_satN_AR.txt	2024/12/5 10:42	文本文档	352 KB
position.txt	2024/12/5 10:42	文本文档	614 KB
ZTDW_Clock.txt	2024/12/5 10:42	文本文档	321 KB

Fig. 24 Result files generated by PPP AR of single station

6.2 Multiple station processing

Combine observation files from multiple stations (*. *o) and the precision clock file (*.CLK), precision orbit file (*.SP3), OSB product file (*.BIA), satellite attitude file (*.OBX) and antenna file (*.atx) are placed in the same folder, as shown in Fig. 25. In the position information configuration interface in Fig. 7, tick the 'Multi-station data processing' box and click the 'Select input data folder path' button to select the folder

where the multi-station observation data is stored. The list of generated folder is shown in Fig. 26.

AREG00PER_R_20230380000_01D_30S_MO.23o	2023/8/21 14:01	23O 文件	33,931 KB
BRDM00DLR_S_20230380000_01D_MN.rnx	2023/2/13 17:45	RNX 文件	7,935 KB
BRUX00BEL_R_20230380000_01D_30S_MO.23o	2023/8/21 14:02	23O 文件	45,037 KB
CEBR00ESP_R_20230380000_01D_30S_MO.23o	2023/8/21 14:02	23O 文件	35,708 KB
DJIG00DJI_R_20230380000_01D_30S_MO.23o	2023/8/21 14:02	23O 文件	51,809 KB
GAMG00KOR_R_20230380000_01D_30S_MO.23o	2023/8/21 14:02	23O 文件	54,840 KB
GBM0MGXRAP_20230380000_01D_05M_ORB.SP3	2023/2/13 17:45	SP3 文件	2,919 KB
GBM0MGXRAP_20230380000_01D_30S_ABS.BIA	2023/2/13 23:53	BIA 文件	252,112 KB
GBM0MGXRAP_20230380000_01D_30S_ATT.OBX	2023/2/13 17:45	OBX 文件	36,984 KB
GBM0MGXRAP_20230380000_01D_30S_CLK.CLK	2023/2/13 17:45	CLK 文件	24,263 KB
HARB00ZAF_R_20230380000_01D_30S_MO.23o	2023/8/21 14:02	23O 文件	44,345 KB
igs20_2221.atx	2023/2/13 17:45	ATX 文件	31,428 KB
KIT300UZB_R_20230380000_01D_30S_MO.23o	2023/12/19 21:09	23O 文件	37,534 KB
KOKV00USA_R_20230380000_01D_30S_MO.23o	2023/12/19 21:09	23O 文件	15,486 KB
LEIJ00DEU_R_20230380000_01D_30S_MO.23o	2023/8/21 14:02	23O 文件	57,016 KB
MAS100ESP_R_20230380000_01D_30S_MO.23o	2023/12/19 21:09	23O 文件	35,619 KB
METG00FIN_R_20230380000_01D_30S_MO.23o	2023/8/21 14:02	23O 文件	44,807 KB
SGOC00LKA_R_20230380000_01D_30S_MO.23o	2023/8/21 14:02	23O 文件	69,854 KB
SUTM00ZAF_R_20230380000_01D_30S_MO.23o	2023/8/21 14:02	23O 文件	56,016 KB
YEL200CAN_R_20230380000_01D_30S_MO.23o	2023/12/19 21:09	23O 文件	41,440 KB

Fig. 25 Multi-station data-processing preparation files

Real_AREG_UC_PPP_GEC_KINEMATI...	2023/12/20 8:57	文件夹
Real_BRUX_UC_PPP_GEC_KINEMATI...	2023/12/20 8:59	文件夹
Real_CEBR_UC_PPP_GEC_KINEMATIC...	2023/12/20 9:00	文件夹
Real_DJIG_UC_PPP_GEC_KINEMATIC...	2023/12/20 9:01	文件夹
Real_GAMG_UC_PPP_GEC_KINEMAT...	2023/12/20 9:03	文件夹
Real_HARB_UC_PPP_GEC_KINEMATI...	2023/12/20 9:04	文件夹
Real_KIT3_UC_PPP_GEC_KINEMATIC...	2023/12/20 9:06	文件夹
Real_LEIJ_UC_PPP_GEC_KINEMATIC...	2023/12/20 9:07	文件夹
Real_MAS1_UC_PPP_GEC_KINEMATI...	2023/12/20 9:08	文件夹
Real_METG_UC_PPP_GEC_KINEMATI...	2023/12/20 9:09	文件夹
Real_AREG_UC_PPP_GEC_KINEMATI...	2023/12/20 9:15	文件夹
Real_BRUX_UC_PPP_GEC_KINEMATI...	2023/12/20 9:16	文件夹
Real_CEBR_UC_PPP_GEC_KINEMATIC...	2023/12/20 9:18	文件夹
Real_DJIG_UC_PPP_GEC_KINEMATIC...	2023/12/20 9:19	文件夹
Real_GAMG_UC_PPP_GEC_KINEMAT...	2023/12/20 9:20	文件夹
Real_HARB_UC_PPP_GEC_KINEMATI...	2023/12/20 9:22	文件夹
Real_KIT3_UC_PPP_GEC_KINEMATIC...	2023/12/20 9:24	文件夹
Real_LEIJ_UC_PPP_GEC_KINEMATIC...	2023/12/20 9:25	文件夹
Real_MAS1_UC_PPP_GEC_KINEMATI...	2023/12/20 9:26	文件夹
Real_METG_UC_PPP_GEC_KINEMATI...	2023/12/20 9:27	文件夹

Fig. 26 Multi-station results folder

6.3 Multi-day data processing

Referring to the contents of the file in Fig. 25, place the data processed over multiple days into separate folders on a day-by-day basis. In the position information configuration interface in Fig. 7, tick the 'Multi-station data processing' box, tick the 'Multi-day data processing', and click the 'Select input data folder path' button to select

the folder where the multi-day observation data is stored.

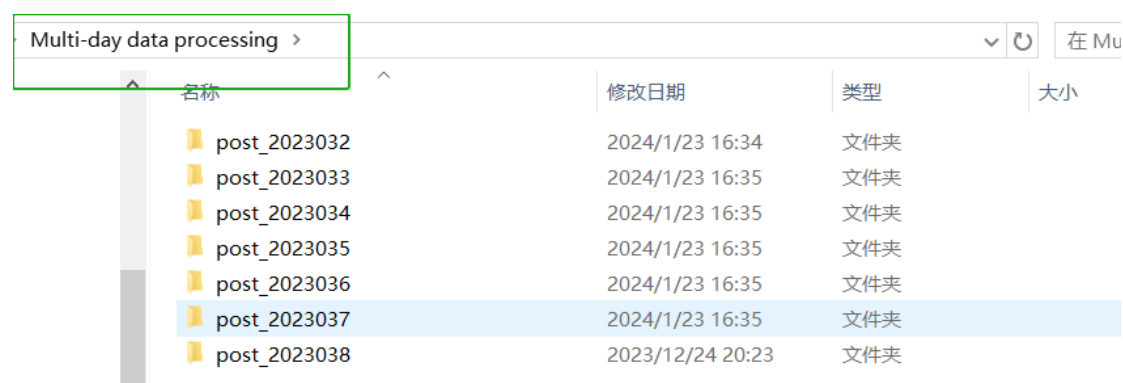


Fig. 27 Folders where multi-day data is stored

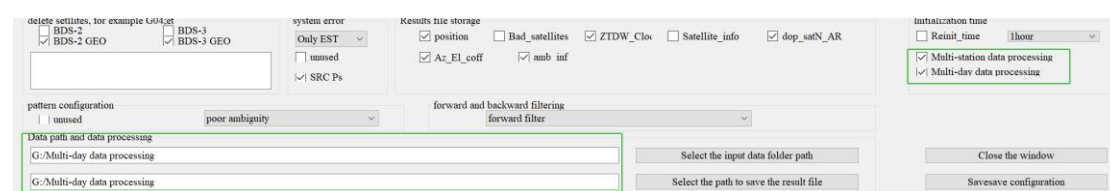


Fig. 28 Multi-day data processing configuration interface

7 Result and analysis

7.1 position.txt and back_position.txt

After processing the data, a position.txt file is generated by MG-MixF PPP AR which saves the epoch number, observation time, number of valid satellites, PPP AR coordinates, and PPP coordinates. The back_position.txt file has the same contents as the position.txt file.

Epoch	Time	Satellite number	PPP AR coordinates
0: 2023-2-1 0: 0: 0.000000	22	1942816.2346	-5804076.5109
1: 2023-2-1 0: 0: 30.000000	23	1942815.0115	-5804075.1208
2: 2023-2-1 0: 1: 0.000000	23	1942816.1838	-5804076.4168
3: 2023-2-1 0: 1: 30.000000	23	1942816.4191	-5804076.6868
4: 2023-2-1 0: 2: 0.000000	24	1942816.4226	-5804077.0767
5: 2023-2-1 0: 2: 30.000000	24	1942816.4313	-5804077.1035
6: 2023-2-1 0: 3: 0.000000	24	1942816.7261	-5804077.4969
7: 2023-2-1 0: 3: 30.000000	24	1942816.5809	-5804077.3743
8: 2023-2-1 0: 4: 0.000000	24	1942816.4564	-5804077.1920
9: 2023-2-1 0: 4: 30.000000	24	1942816.4554	-5804077.1957
10: 2023-2-1 0: 5: 0.000000	24	1942816.5674	-5804077.0843
11: 2023-2-1 0: 5: 30.000000	24	1942816.4054	-5804077.1300
12: 2023-2-1 0: 6: 0.000000	24	1942816.4130	-5804077.3271
13: 2023-2-1 0: 6: 30.000000	23	1942816.4587	-5804077.2043
14: 2023-2-1 0: 7: 0.000000	23	1942816.4581	-5804077.2041
15: 2023-2-1 0: 7: 30.000000	23	1942816.4605	-5804077.2106
16: 2023-2-1 0: 8: 0.000000	23	1942816.4592	-5804077.2069
17: 2023-2-1 0: 8: 30.000000	23	1942816.4571	-5804077.2056
18: 2023-2-1 0: 9: 0.000000	23	1942816.4585	-5804077.2032
19: 2023-2-1 0: 9: 30.000000	23	1942816.4575	-5804077.2014
20: 2023-2-1 0: 10: 0.000000	23	1942816.4581	-5804077.2080
21: 2023-2-1 0: 10: 30.000000	23	1942816.4588	-5804077.2023
22: 2023-2-1 0: 11: 0.000000	23	1942816.4575	-5804077.2023
23: 2023-2-1 0: 11: 30.000000	23	1942816.4586	-5804077.2005
24: 2023-2-1 0: 12: 0.000000	23	1942816.4579	-5804077.2011
25: 2023-2-1 0: 12: 30.000000	23	1942816.4561	-5804077.1942
26: 2023-2-1 0: 13: 0.000000	23	1942816.4561	-5804077.1945
27: 2023-2-1 0: 13: 30.000000	24	1942816.4577	-5804077.2051
28: 2023-2-1 0: 14: 0.000000	24	1942816.4548	-5804077.1987
29: 2023-2-1 0: 14: 30.000000	24	1942816.4559	-5804077.1940
30: 2023-2-1 0: 15: 0.000000	24	1942816.4563	-5804077.1987

Fig. 29 Screenshot of position.txt file

7.2 Ambiguity_information.txt and back_Ambiguity_information.txt

After selecting to output the Ambiguity_information.txt file and completing the data

processing, MG-MixF PPP AR outputs the number of calendar elements, the observation time, the reference satellites, the number of successfully fixed ambiguities, and the ratio value after the LAMBDA search to the file. In addition, the elevation, ionospheric delay, cycle slip flag, float ambiguities, fixed ambiguities, and covariance matrix corresponding to narrow lane ambiguities for each satellite involved in the solution are also output in the Ambiguity_information.txt file. The character position of each column is shown in Table 1. The screenshot of Ambiguity_information.txt file shown in Fig. 30. The back_Ambiguity_information.txt file has the same contents as the Ambiguity_information.txt file.

Table 1 Ambiguity_information.txt format description

items	value type	Beginning and ending bytes
Satellite system type	char	1-1
Satellite PRN	int	2-3
Satellite elevation	double	6-10
Cycle slip flag	int	17-17
Ionospheric delay	double	24-29
Extra-wide lane ambiguity smoothing length	int	36-40
Extra-wide lane BSSD (Between-Satellite Single-Difference) float ambiguity	double	42-48
Extra-wide lane BSSD fixed ambiguity	int	51-54
Extra-wide lane ambiguity smoothing length	int	61-65
Extra-wide lane BSSD float ambiguity	double	67-73
Extra-wide lane BSSD fixed ambiguity	int	76-79
Extra-wide lane ambiguity smoothing length	int	86-90
Extra-wide lane BSSD float ambiguity	double	92-98
Extra-wide lane BSSD fixed ambiguity	int	101-104
Wide lane ambiguity smoothing length	int	111-115
Wide lane BSSD float ambiguity	double	117-123
Wide lane BSSD fixed ambiguity	int	126-129

double 138-143

Fig. 30 Screenshot of Ambiguity information.txt file

After selecting to output the dop_satN_AR.txt file and completing the data processing, MG-MixF PPP AR outputs the number of calendar elements, the observation time, number of valid satellites, the GDOP value, the PDOP value, the HDOP value, the VDOP value, the ratio value, the number of fixed ambiguities. The screenshot of dop_satN_AR.txt file shown in Fig. 31. The back_dop_satN_AR.txt file has the same contents as the dop_satN_AR.txt file.

Fig. 31 Screenshot of dop satN AR.txt file

After selecting to output the Az_El_coff.txt file and completing the data processing, MG-MixF PPP AR outputs the number of calendar elements, the observation time, the valid satellites, the azimuth, the elevation. The screenshot of Az_El_coff.txt file shown in Fig. 31. The back_Az_El_coff.txt file has the same contents as the Az_El_coff.txt file.

				azimuth	elevation
4	0:	2023-02-07 00:00:00.00	E24	70.67	67.35
5	0:	2023-02-07 00:00:00.00	E25	345.91	33.86
6	0:	2023-02-07 00:00:00.00	E31	132.60	30.29
7	0:	2023-02-07 00:00:00.00	E34	262.21	20.28
8	0:	2023-02-07 00:00:00.00	E36	317.63	27.06
9	1:	2023-02-07 00:00:30.00	C23	278.98	76.65
10	1:	2023-02-07 00:00:30.00	C25	150.27	45.56
11	1:	2023-02-07 00:00:30.00	C32	212.79	22.07
12	1:	2023-02-07 00:00:30.00	C33	70.17	38.78
13	1:	2023-02-07 00:00:30.00	C37	314.12	26.30
14	1:	2023-02-07 00:00:30.00	C41	157.14	63.72
15	1:	2023-02-07 00:00:30.00	E04	86.78	10.52
16	1:	2023-02-07 00:00:30.00	E05	203.12	36.03
17	1:	2023-02-07 00:00:30.00	E09	132.09	42.33
18	1:	2023-02-07 00:00:30.00	E24	71.19	67.44
19	1:	2023-02-07 00:00:30.00	E25	345.89	34.05
20	1:	2023-02-07 00:00:30.00	E31	132.75	30.16
21	1:	2023-02-07 00:00:30.00	E34	262.41	20.24
22	1:	2023-02-07 00:00:30.00	E36	317.79	26.93
23	1:	2023-02-07 00:00:30.00	G05	216.60	14.64

Fig. 32 Screenshot of Az_El_coff.txt file

7.5 ZTDW_Clock.txt and back_ZTDW_Clock.txt

After selecting to output the ZTDW_Clock.txt file and completing the data processing, MG-MixF PPP AR outputs the number of calendar elements, the observation time, the zenith wet tropospheric delay, the GPS receiver clock, the BDS-2 receiver clock, the BDS-3 receiver clock, the GLONASS receiver clock, the Galileo receiver clock. The screenshot of ZTDW_Clock.txt file shown in Fig. 33. The back_ZTDW_Clock.txt file has the same contents as the ZTDW_Clock.txt file.

epoch	Observation time	ZTD(m)	base_clk_G(m)	diff_clk_C2(m)	diff_clk_C3(m)	diff_clk_R(m)
0: 2023- 2- 7 0: 0: 0.000000	0.3453	0.0000	0.0000	0.0000	0.0000	-124782.9832
1: 2023- 2- 7 0: 0:30.000000	0.3439	-124781.6379	0.0000	-124776.6612	0.0000	-124781.5344
2: 2023- 2- 7 0: 1: 0.000000	0.3410	-124782.3528	0.0000	-124777.6074	0.0000	-124781.8167
3: 2023- 2- 7 0: 1:30.000000	0.3254	-124782.7528	0.0000	-124778.0735	0.0000	-124782.0312
4: 2023- 2- 7 0: 2: 0.000000	0.2810	-124782.8859	0.0000	-124778.3495	0.0000	-124782.2082
5: 2023- 2- 7 0: 2:30.000000	0.2634	-124783.0575	0.0000	-124778.6219	0.0000	-124782.3344
6: 2023- 2- 7 0: 3: 0.000000	0.2178	-124782.9171	0.0000	-124778.3764	0.0000	-124782.1640

Fig. 33 Screenshot of ZTDW_Clock.txt file

7.6 bad_satellites.txt and back_bad_satellites.txt

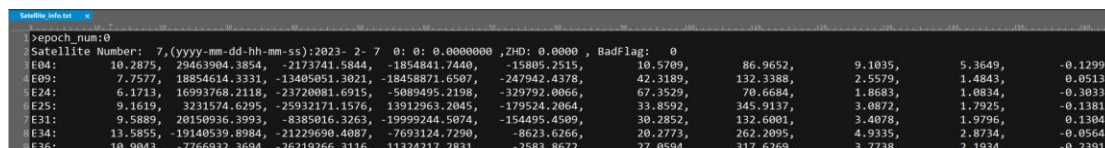
MG-MixF PPP AR will store satellites not participating in the calculation in the bad_satellites.txt file, which mainly contains epoch number, satellite number, observation time, and abnormal information. The bad_satellites.txt file format is presented in Fig. 34. The back_bad_satellites.txt file has the same contents as the bad_satellites.txt file.

epoch	satellite number	Observation time	abnormal information
0: G30 2023- 2- 7 0: 0: 0.000000	Eliminate info: PHASE_BIA	CODE_BIA is not	---ppp_model\uduc_ppp_ar.cpp, line:361, fuction:uduc_ppp_ar_calculating
0: G20 2023- 2- 7 0: 0: 0.000000	Eliminate info: PHASE_BIA	CODE_BIA is not	---ppp_model\uduc_ppp_ar.cpp, line:361, fuction:uduc_ppp_ar_calculating
0: G14 2023- 2- 7 0: 0: 0.000000	Eliminate info: PHASE_BIA	CODE_BIA is not	---ppp_model\uduc_ppp_ar.cpp, line:361, fuction:uduc_ppp_ar_calculating
0: G11 2023- 2- 7 0: 0: 0.000000	Eliminate info: PHASE_BIA	CODE_BIA is not	---ppp_model\uduc_ppp_ar.cpp, line:361, fuction:uduc_ppp_ar_calculating
0: G09 2023- 2- 7 0: 0: 0.000000	Eliminate info: PHASE_BIA	CODE_BIA is not	---ppp_model\uduc_ppp_ar.cpp, line:361, fuction:uduc_ppp_ar_calculating
0: G07 2023- 2- 7 0: 0: 0.000000	Eliminate info: PHASE_BIA	CODE_BIA is not	---ppp_model\uduc_ppp_ar.cpp, line:361, fuction:uduc_ppp_ar_calculating

Fig. 34 Screenshot of bad_satellites.txt file

7.7 Satellite_info.txt and back_Satellite_info.txt

MG-MixF PPP AR will store satellites not participating in the calculation in the Satellite_info.txt file, which mainly contains epoch number, satellite number, observation time, ionospheric delay, satellite orbits and clock, azimuth and altitude angles of satellites, tropospheric delay and map function coefficients, relativistic correction, sagnac correction, tidal correction, antenna height correction, satellite antenna correction, receiver antenna correction, phase wind-up correction, etc. The Satellite_info.txt file format is presented in Fig. 35. The back_Satellite_info.txt file has the same contents as the Satellite_info.txt file.



```

>epoch_num:0
Satellite Number: 7,(yyyy-mm-dd-hh-mm-ss):2023- 2- 7  0: 0: 0.0000000 ,ZHD: 0.0000 , BadFlag:  0
E04:  10.2875, 29463904.3854, -2173741.5844, -1854841.7440, -15805.2515, 10.5709, 86.9652, 9.1835, 5.3649, -0.1299,
E09:  7.7577, 18854614.3331, -13405051.3021, -18458871.6507, -247942.4378, 42.3189, 132.3388, 2.5579, 1.4843, 0.0513,
E24:  6.1713, 16993768.2118, -23720081.6915, -5089495.2198, -329792.0066, 67.3529, 70.6684, 1.8683, 1.0834, -0.3033,
E25:  9.1619, 3231574.6295, -25932171.1576, 13912963.2045, -179524.2064, 33.8592, 345.9137, 3.0872, 1.7925, -0.1381,
E31:  9.5889, 20150936.3993, -8385016.3263, -19999244.5074, -154495.4509, 30.2852, 132.6001, 3.4078, 1.9796, 0.1304,
E34:  13.5855, -19140539.8984, -21229690.4087, -7693124.7290, -8623.6266, 20.2773, 262.2095, 4.9335, 2.8734, -0.0564,
E36:  10.9043, -7766932.3694, -26219266.3116, 11324217.2831, -2583.8672, 27.0594, 317.6269, 3.7738, 2.1934, -0.2391,

```

Fig. 35 Screenshot of Satellite_info.txt file

8 Thanks & Support

We would like to thank the IGS, CNES, and GFZ for providing GNSS data and orbit and clock products. We also express our sincere gratitude to some of the software sources listed below.

Software:

Qt: <www.qt.io>

Eigen: <eigen.tuxfamily.org>

RTKLIB: <www.rtklib.com>

MG-APP: <https://github.com/xiaogongwei/MG_APP>

Appendix

A. Data processing models and strategies of MG-MixF PPP-AR

Currently, several universities and research institutes have released satellite-side OSB products. The CNES generates multi-frequency OSB solutions in SINEX format to support multi-frequency uncombined GPS, Galileo, and BDS PPP-AR (Gazzino et al. 2023). The WHU provides phase clock and OSB products supporting GPS, Galileo, and BDS PPP-AR (Geng et al. 2019). Meanwhile, CODE's final precise ephemeris and OSB products support GPS and Galileo PPP-AR (Schaer et al. 2021). Table 2 outlines the processing strategy for the static and kinematic experiments. Note that Geostationary Earth Orbit (GEO) satellites of BDS are excluded due to the poor accuracy of their orbit products. The positioning error is defined as the difference between the positioning solution and the reference solution. The positioning accuracy is the root mean square (RMS) of converged positioning errors. The mean RMS is defined as the average of all daily RMS values for all station. The TTFF is defined as the time required to obtain the first correct fixed solution, and the positioning error of fixed solution is less than that of float solution at the same instant. The definition of convergence time is that the horizontal positioning solutions are less than 10cm for at least 5 min. The fixing rate is the ratio of the fixed epochs number to the total epochs number.

Table 2 Data processing models and strategies of BDS/GPS/Galileo PPP-AR

Item	Strategy
Software	MG-MixF PPP-AR
PPP model	Undifferenced and uncombined PPP
Observations of tri-frequency	BDS-3: B1I/B3I/B2a, GPS: L1/L2/L5, Galileo: E1/E6/E5a
Observations of dual-frequency	GPS: L1/L2; BDS: B1I/B3I; Galileo: E1/E5a
Cut-off elevation angle	10°
Satellite orbit/clock	WHU rapid precise orbit and clock products
Satellite code and carrier phase OSB	WHU OSB products

Observation weight	Elevation-dependent weighting
Receiver clocks	Single-epoch white noise estimation with a priori was 10,000 m
Inter-system biases	Random walk estimation (Zhou et al. 2019)
Tri-frequency receivers IFB	The prior accuracy was 10,000 m
Tropospheric zenith hydrostatic delay	UNB3m/Saastamoinen (GPT2)(Böhm et al. 2015)
Zenith wet tropospheric delay	Mapping function: GMF; modeled by a random walk estimation with system noise $2.5 \times 10^{-11} m^2 / s$ (Liu et al. 2021)
Slant ionosphere delay parameters	The prior accuracy was 20m
PCO/PCV	igs14_2221.atx(Sl et al. 2021)
Receiver position	Static (Estimated as constants), kinematic (Estimated as white noise (1e6))
Ambiguity parameters	Constant and random walk
Parameter estimator	SRIF filter
Reference satellite	Maximum elevation angle satellite
Three-frequency ambiguity fixing	Extra wide lane(EWL), wide lane(WL), narrow lane (NL) LAMBDA algorithm (Tao et al. 2022)
Ratio test	2.0(Leick et al. 2015)

B. The urban and ocean Kinematic Experiment

Table 3 summarizes the basic information of kinematic experiments. Fig. 36 shows the reference station position and vehicle trajectory, where the longest baseline between the reference station and the vehicle is 10 km. The true value is the ambiguity-fixed solution of GLONASS/GPS combined RTK calculated by Inertial Explorer 8.90 software.



Fig. 36 Vehicle track of urban kinematic experiment.

Table 3 Basic information of the experiment in urban areas

Experiment	Information
Starting time	2023, 196, GPS time 07:48:08

Ending time	2023, 196, GPS time 09:16:29
Sampling interval (s)	1
Rover station receiver	OEM729
Rover station antenna	Harxon HX-CSX601A

To further validate its advantages at ocean, we conducted ocean experiments. The trajectory of the ocean platform data is shown in Fig. 37. The HKMW acts as the reference station with a maximal baseline distance of 30 km to the vessel, located in Hong Kong, China. The sampling time is from 06:30:41 to 07:41:07 on August 29, 2023.



Fig. 37 Reference station position, experimental equipment, and ocean tracking in kinematic experiment.

C. Methods

For a user receiver r tracking the satellite s of a constellation g , indicating GPS, BDS, and Galileo system, at frequency j ($j = 1, 2, 3$), the functional model of pseudo-range and carrier phase observation equations can be formulated as:

$$\begin{aligned} P_{r,j}^{s,g} &= \rho_r^{s,g} + M_r^{s,g} Z_w + dt_r - d\tau^{s,g} + \gamma_j^g I_r^{s,g} + d_{r,j}^g - d_j^{s,g} + \varepsilon_{P_{r,j}^{s,g}} \\ L_{r,j}^{s,g} &= \rho_r^{s,g} + M_r^{s,g} Z_w + dt_r - d\tau^{s,g} - \gamma_j^g I_r^{s,g} + b_{r,j}^g - b_j^{s,g} + \lambda_j^g N_{r,j}^{s,g} + \varepsilon_{L_{r,j}^{s,g}} \end{aligned} \quad (1)$$

The symbols P and L denotes pseudo-range and carrier phase observations in meters, respectively, and their noises are ε_p and ε_L in meters, respectively; ρ is the geometric distance between receiver antenna carrier phase center and carrier phase satellite antenna carrier phase center in meters; Z_w is the wet part of slant tropospheric delay in the zenith direction in meters, M_r is the mapping function of zenith wet delay Z_w ;

c is the speed of light; dt and $d\tau$ are respectively the clock offsets of receiver and satellite in meters; I is the slant ionospheric delay in meters, $\gamma_j^g = (f_1^g / f_j^g)^2$ is factor at the frequency f_j^g ; d_r and d^s are the pseudo-range hardware delay bias of satellite- and receiver-side in meters, respectively; λ_j^g is the wavelength of the phase observation; N is the undifferenced integer ambiguity in cycles; b_r and $b^{s,g}$ are respectively the initial phase bias and hardware delay bias of satellite- and receiver-side in meter. For a brief, the errors ignored in equation gross errors1) including carrier phase wind-up, tidal displacements, earth rotation, and relativistic effects can be corrected using existing models.

Precise orbit and clock products are used to achieve precise point positioning. The uncombined and undifferenced measurements are used directly in the raw observation approach. The pseudo-range and carrier phase observations hardware delay bias of satellite- and receiver-side are not estimable in a single receiver, a reparameterization is therefore needed. Taking the fact that satellite clock combined with additional observable-specific signal biases (OSBs) product can correct satellite-side initial phase bias and hardware delay bias. The raw observation equation of can be formed as follows:

$$\begin{aligned}\delta P_{r,j}^{s,g} &= \mu_r^{s,g} \Delta x_r + M_r^{s,g} Z_w + dt_r^g + \gamma_j^g \tilde{I}_r^{s,g} + F_{r,j}^g \\ \delta L_{r,j}^{s,g} &= \mu_r^{s,g} \Delta x_r + M_r^{s,g} Z_w + dt_r^g - \gamma_j^g \tilde{I}_r^{s,g} + \lambda_j^g \tilde{N}_{r,j}^{s,g}\end{aligned}$$

where $\delta P_{r,j}^{s,g}$ and $\delta L_{r,j}^{s,g}$ are Observed Minus Computed (OMC) values. These are calculated from raw observations and a priori coordinates, as well as the precise satellite orbit and clock. $\mu_r^{s,g}$ is the LOS between the receiver and the satellite, whereas Δx_r is the increment of the receiver position relative to the initial position, $F_{r,j}^g$ is the inter-frequency code bias for multi-frequency pseudo-range observation($j < 3, F = 0$).

In order to realize the fixed ambiguity, the hardware delay deviation in the receiver side of the ambiguity parameter needs to be eliminated by BSSD. In the process of BSSD, the satellite with the highest altitude Angle among the satellites with the most observation frequency is selected as the reference satellite.

The observation equations for all observed satellites of one constellation in the matrix-vector form is expressed as:

$$E \begin{bmatrix} \mathbf{P}^1 \\ \Phi^1 \\ \vdots \\ \mathbf{P}^m \\ \Phi^m \end{bmatrix} = \begin{bmatrix} H^1 & M^1 & \Gamma^1 & & E^1 & \\ \vdots & \vdots & & \ddots & & \\ & & & & \ddots & \\ H^m & M^m & & \Gamma^m & & E^m \end{bmatrix} \begin{bmatrix} \mathbf{x}_r \\ \mathbf{t}_r \\ \mathbf{I} \\ \mathbf{N}_r^s \end{bmatrix}$$

Where m is the number of satellites in the current epoch; H^m contains the unit vectors of LOS (Line of Sight) and the mapping function value of zenith delay of troposphere, the parameter coefficient matrix is as follows:

$$\mathbf{H}^m = \begin{bmatrix} \Delta l_{1,r}^{m,s} & \Delta l_{1,r}^{m,s} & \Delta l_{2,r}^{m,s} & \Delta l_{2,r}^{m,s} & \Delta l_{3,r}^{m,s} & \Delta l_{3,r}^{m,s} \\ \Delta m_{1,r}^{m,s} & \Delta m_{1,r}^{m,s} & \Delta m_{2,r}^{m,s} & \Delta m_{2,r}^{m,s} & \Delta m_{3,r}^{m,s} & \Delta m_{3,r}^{m,s} \\ \Delta n_{1,r}^{m,s} & \Delta n_{1,r}^{m,s} & \Delta n_{2,r}^{m,s} & \Delta n_{2,r}^{m,s} & \Delta n_{3,r}^{m,s} & \Delta n_{3,r}^{m,s} \\ -Mw_{1,r}^{m,s} & -Mw_{1,r}^{m,s} & -Mw_{2,r}^{m,s} & -Mw_{2,r}^{m,s} & -Mw_{3,r}^{m,s} & -Mw_{3,r}^{m,s} \end{bmatrix}^T$$

and the parameter $\mathbf{x}_r = [\Delta x \ \Delta y \ \Delta z \ ZWD_r]^T$. When the satellite system is GPS, the matrix \mathbf{M}^m is expressed as follows:

$$\mathbf{M}^m = \begin{bmatrix} -1 & -1 & -1 & -1 & -1 & -1 \\ 0 & 0 & 0 & 0 & -1 & -1 \\ 0 & 0 & 0 & 0 & 0 & 0 \\ 0 & 0 & 0 & 0 & 0 & 0 \\ 0 & 0 & 0 & 0 & 0 & 0 \\ 0 & 0 & 0 & 0 & 0 & 0 \end{bmatrix}^T$$

with the parameter $\mathbf{t}_r = [cd\bar{t}_{r,G} \ IFB_G \ cd\bar{t}_{r,E} \ IFB_E \ cd\bar{t}_{r,C} \ IFB_C]^T$, where IFB is inter-frequency bias, the number of inter-frequency bias in each system is $j-2$, when the mixed frequency number $j \leq 2$, there is no IFB in \mathbf{t}_r ; j is number of frequencies used by each satellite.

Where $\Gamma^m = \left[\left(\frac{f_1^m}{f_1^m} \right)^2 - \left(\frac{f_1^m}{f_1^m} \right)^2 \quad \left(\frac{f_1^m}{f_2^m} \right)^2 - \left(\frac{f_1^m}{f_2^m} \right)^2 \quad \left(\frac{f_1^m}{f_3^m} \right)^2 - \left(\frac{f_1^m}{f_3^m} \right)^2 \right]^T$ with the

$$\text{parameter} \quad \mathbf{I} = \begin{bmatrix} I^{1,s} & \cdots & I^{m,s} \end{bmatrix} \quad . \quad \mathbf{E}^m = \begin{bmatrix} 0 & \lambda_1^m & 0 & 0 & 0 & 0 \\ 0 & 0 & 0 & \lambda_2^m & 0 & 0 \\ 0 & 0 & 0 & 0 & 0 & \lambda_3^m \end{bmatrix}^T \quad \text{and}$$

$$\mathbf{N}_r^s = \begin{bmatrix} N_r^{1,s} & \cdots & N_r^{m,s} \end{bmatrix}.$$

Residual vector of observations \mathbf{L} :

$$\mathbf{L} = \begin{bmatrix} \rho - P^1 + \Delta^1 \\ \rho - L^1 + \Delta^1 \\ \vdots \\ \rho - P^n + \Delta^n \\ \rho - L^n + \Delta^n \end{bmatrix}$$

where ρ is the calculated pseudo distance; P^n is the pseudo-distance observation value; L^n is the observed carrier phase; Δ^n is the correction of satellite clock difference, tropospheric zenith dry delay, relativity, earth rotation effect, tidal effect and antenna center shift.

Noise covariance matrix of observations \mathbf{R} :

$$\mathbf{R} = \begin{bmatrix} \sigma_{p_1}^1 & & & & \\ & \sigma_{l_1}^1 & & & \\ & & \ddots & & \\ & & & \sigma_{p_3}^n & \\ & & & & \sigma_{l_3}^n \end{bmatrix}$$

where σ_p^n is about the pseudo-distance observation noise, is about the carrier phase observation noise. σ_l^n is about the carrier phase observation noise. The stochastic model is based on the height Angle; n is the sum of all frequencies of all satellites. By linear transformation of the state transition matrix \mathbf{F} , to perform a fixed calculation of the required ambiguity.

When the available frequency of the satellite is less than 3, the satellite ambiguity is not fixed and the floating point solution is adopted. The longest wavelength after WL combination is found as EWL, the shortest wavelength is used as WL, and the IF combination is used as NL, and then the BSSD ambiguity is fixed step by step (EWL, WL, NL) through the cascaded ambiguity fixing method. First, the EWL is fixed as an

integer, and the remaining parameters of the remaining matrix are updated, and then the WL is fixed as an integer and other parameters are updated again. Finally, the integer solution of NL ambiguity is determined by the difference between EWL ambiguity and WL ambiguity by floating point ambiguity.

In this method, the elements in the design matrix are slightly processed, and the original ambiguity in L2 observation is decomposed into WL and NL ambiguity, and the original ambiguity in L3 observation is decomposed into EWL, WL and NL ambiguity:

The three-frequency non-difference non-combination PPP fixed solution is obtained by fixing the BSSD extra-wide lane, wide lane, and NL ambiguities degree successively through the cascade fuzzy degree fixing method. The state vector and variance of the three-frequency non-difference non-combined PPP floating-point resolution ambiguity between stars are:

$$\tilde{\mathbf{x}} = A\hat{\mathbf{x}}, Q_{\tilde{\mathbf{x}}\tilde{\mathbf{x}}} = A Q_{\hat{\mathbf{x}}\hat{\mathbf{x}}} A^T$$

$$\tilde{\mathbf{x}} = \begin{bmatrix} \tilde{\mathbf{x}}_1 \\ \tilde{\mathbf{x}}_2 \\ \tilde{\mathbf{x}}_3 \\ \tilde{\mathbf{x}}_4 \end{bmatrix}, Q_{\tilde{\mathbf{x}}\tilde{\mathbf{x}}} = \begin{bmatrix} Q_{11} & Q_{12} & Q_{13} & Q_{14} \\ Q_{21} & Q_{22} & Q_{23} & Q_{24} \\ Q_{31} & Q_{32} & Q_{33} & Q_{34} \\ Q_{41} & Q_{42} & Q_{43} & Q_{44} \end{bmatrix}$$

where, $\tilde{\mathbf{x}}$ is the single difference state vector between stars, $Q_{\tilde{\mathbf{x}}\tilde{\mathbf{x}}}$ is the variance covariance matrix of $\tilde{\mathbf{x}}$; $\hat{\mathbf{x}}$ is a floating-point solution state vector; A is the BSSD state transition matrix of the maximum elevation angle satellite as the reference star. The state vector $\tilde{\mathbf{x}}_4$ is formed by BSSD EWL ambiguities $\tilde{N}_{r,EWL}^{st,g}$. BSSD EWL ambiguity $\tilde{N}_{r,WL}^{st,g}$ is composed of state vector $\tilde{\mathbf{x}}_3$; Inter-star single difference NL ambiguity $\tilde{N}_{r,I}^{st,g}$ is composed of state vector $\tilde{\mathbf{x}}_2$, position, zenith tropospheric wet delay, ionosphere, receiver clock difference and so on are composed of $\tilde{\mathbf{x}}_1$.

$$\tilde{\mathbf{x}}_{1,2} = \hat{\mathbf{x}}_{1,2} - Q_{13,23} (Q_{33})^{-1} (\tilde{\mathbf{x}}_3 - \tilde{\mathbf{x}}_3)$$

$$Q_{\tilde{\mathbf{x}}_{1,2}} = Q_{\hat{\mathbf{x}}_{1,2}} - Q_{13,23} (\hat{Q}_{33})^{-1} (Q_{13,23})^T$$

$$\hat{\mathbf{x}}_{1,2} = \begin{bmatrix} \hat{\mathbf{x}}_1 \\ \hat{\mathbf{x}}_2 \end{bmatrix}, Q_{13,23} = \begin{bmatrix} \hat{Q}_{13} \\ \hat{Q}_{23} \end{bmatrix}, Q_{\hat{\mathbf{x}}_{1,2}} = \begin{bmatrix} \hat{Q}_{11} & \hat{Q}_{12} \\ \hat{Q}_{21} & \hat{Q}_{22} \end{bmatrix}$$

$$\bar{\mathbf{x}}_{1,2} = \begin{bmatrix} \bar{\mathbf{x}}_1 \\ \bar{\mathbf{x}}_2 \end{bmatrix}, Q_{\bar{\mathbf{x}}_{1,2}} = \begin{bmatrix} \bar{Q}_{11} & \bar{Q}_{12} \\ \bar{Q}_{21} & \bar{Q}_{22} \end{bmatrix}$$

The float ambiguity and variance of the updated inter-star single difference NL with fixed integer ambiguity in the fixed width of the inter-star single difference are put into the LAMBDA function to search for the inter-star single difference NL integer ambiguity candidate. When the global ambiguity fails to be fixed, the integer ambiguity solution of NL with partial ambiguity fixing is considered. Once the ambiguity is successfully fixed to an integer, the state vectors $\bar{\mathbf{x}}_i$ and their variance-covariance matrix can be updated by fixed-minus-float ambiguity increments, as shown in the following formula:

$$\bar{\mathbf{x}}_1 = \hat{\mathbf{x}}_1 - \bar{Q}_{12} (\bar{Q}_{22})^{-1} (\bar{\mathbf{x}}_2 - \hat{\mathbf{x}}_2)$$

$$Q_{\bar{\mathbf{x}}_1} = \bar{Q}_{11} - \bar{Q}_{12} (\bar{Q}_{22})^{-1} (\bar{Q}_{12})^T$$

Finally, the position solution vector $\bar{\mathbf{x}}_i$ after fixed ambiguity update is obtained.

References

- Böhm J, Möller G, Schindelegger M, Pain G, Weber R. Development of an improved empirical model for slant delays in the troposphere (GPT2w). *GPS Solutions*, 2015, 19: 433-441
- Gazzino C, Blot A, Bernadotte E, Jayle T, Laymand M, Lelarge N, Lacabanne A, Laurichesse D, Kos S, Fernandez J, Prieto J F. The CNES Solutions for Improving the Positioning Accuracy with Post-Processed Phase Biases, a Snapshot Mode, and High-Frequency Doppler Measurements Embedded in Recent Advances of the PPP-WIZARD Demonstrator. *Remote Sensing*, 2023, 15:
- Geng J, Chen X, Pan Y, Zhao Q. A modified phase clock/bias model to improve PPP ambiguity resolution at Wuhan University. *Journal of Geodesy*, 2019, 2053-2067
- Leick A, Rapoport L, Tatarnikov D. *GPS Satellite Surveying*. 2015.
- Liu T, Chen H, Chen Q, Jiang W, Laurichesse D, An X, Geng T. Characteristics of phase bias from CNES and its application in multi-frequency and multi-GNSS precise point positioning with ambiguity resolution. *GPS Solutions*, 2021, 25: 58
- Schaer S, Villiger A, Arnold D, Dach R, Prange L, Jäggi A. The CODE ambiguity-fixed clock and phase bias analysis products: generation, properties, and performance. *Journal of Geodesy*, 2021, 95: 81
- Sl A, Sb B, Jg C, Ss D. Exchanging satellite attitude quaternions for improved GNSS data processing consistency. *Adv Space Res*, 2021,
- Tao J, Chen G, Guo J, Zhang Q, Liu S, Zhao Q. Toward BDS/Galileo/GPS/QZSS triple-frequency PPP instantaneous integer ambiguity resolutions without atmosphere corrections. *GPS Solutions*, 2022, 26: 127
- Zhou F, Dong D, Li P, Li X, Schuh H. Influence of stochastic modeling for inter-system biases on multi-GNSS undifferenced and uncombined precise point positioning. *GPS Solutions*, 2019, 23: 59